THE ASTROPHYSICAL JOURNAL, 460:735–743, 1996 April 1

OSSE OBSERVATIONS OF THE VELA AND GEMINGA PULSARS

M. S. STRICKMAN,[1] J. E. GROVE, W. N. JOHNSON, R. L. KINZER, R. A. KROEGER, AND J. D. KURFESS
Naval Research Laboratory, Washington, DC 20375-5352
D. A. GRABELSKY, S. M. MATZ, W. R. PURCELL, AND M. P. ULMER
Northwestern University, Evanston, IL 60208
AND
G. V. JUNG
Universities Space Research Association, Washington, DC 20024
Received 1995 March 28; accepted 1995 October 3

ABSTRACT

The Oriented Scintillation Spectrometer Experiment (OSSE) on board the *Compton Gamma Ray Observatory* detected the Vela pulsar (PSR B0833−45) during 1991 August–September, 1992 April–May, and 1993 August. Observed light curves have a two-peak pulse profile similar to that observed at higher energies, although the second peak may be wider in the OSSE light curve. Pulsed emission in the first gamma-ray peak was detected with 4.6 σ statistical significance in the 0.07–0.6 MeV band in the sum of all three observing periods. The second gamma-ray peak was detected at no more than 3 σ significance in the same band. Due to the low statistical significance of the observations, little can be said concerning longer term temporal variability. The spectrum is hard at lower energies and, in combination with higher energy data, appears to require a break in the 20 MeV region. OSSE also observed Geminga during 1992 July, 1993 December, and 1994 July. No significant pulsed emission was observed on any occasion. Upper limits to the pulsed emission suggest, but do not require, a break from the extrapolation of the spectrum measured at higher energies.

Subject headings: gamma rays: observations — pulsars: individual (Vela Pulsar, Geminga)

1. INTRODUCTION

The number of known gamma-ray pulsars has, over the past few years, increased from two (Crab and Vela) to seven with the addition of PSR B1509−58, PSR B1706−44, PSR B1055−52, PSR B1951+32, and the discovery that the gamma-ray object Geminga is a pulsar (Halpern & Holt 1992). The Oriented Scintillation Spectrometer Experiment (OSSE) on board *Compton Gamma Ray Observatory* (*CGRO*) has previously reported detections of the Crab pulsar (Ulmer et al. 1994) and PSR B1509−58 (Matz et al. 1994). We report here on OSSE observations of Vela and Geminga. Neither of these objects is known as a bright hard X-ray or low-energy gamma-ray emitter, although both are relatively nearby and both are intense sources of gamma rays above 100 MeV.

The Vela pulsar (PSR B0833−45), with a period of 0.089 s, is the brightest extrasolar object in the gamma-ray sky at energies above 100 MeV. It has been observed extensively at these energies by *SAS 2* (Thompson et al. 1977), *COS B* (Bennett et al. 1977; Grenier, Hermsen, & Clear 1988), and EGRET (Kanbach et al. 1994). In addition to radio emission, the Vela pulsar also emits faint optical (Wallace et al. 1977) and soft X-ray pulsations (Ögelman, Finley, & Zimmermann 1993). While the radio light curve exhibits a single peak, the gamma-ray light curve is double peaked, with the first peak lagging the radio peak by ~0.11 in phase and the two gamma-ray peaks separated in phase by ~0.42.

The pulsed X-ray spectrum, detected by *ROSAT*, was initially reported (Ögelman et al. 1993) to be consistent with thermal emission at or near the neutron star surface rather than emission from an $e^{\pm}$ cascade in the magnetosphere, the presumed emission mechanism at other observed frequencies. A more recent interpretation (Ögelman 1993) suggests that the total spectrum from the point source colocated with the pulsar can also be modeled by soft and hard components, the latter of which may indicate a magnetospheric contribution. However, the pulsed spectrum is still best represented by a soft blackbody spectrum and is primarily observed below 1 keV. The light curve at soft X-ray energies consists of a broad feature (suggested by Ögelman 1993 to be a double pulse) lagging the radio pulse by approximately 0.5 in phase. The centroid of the broad X-ray peak leads the second gamma-ray peak as shown by Kanbach et al. (1994) by ~0.1 in phase (see Fig. 2 below).

Until recently, Vela has been an elusive target in the hard X-ray and low-energy gamma-ray bands. An observation of 0.3–30 MeV pulsed emission was reported by Tümer et al. (1984) 31 days after a major pulsar period glitch, but negative results have been reported by Ulmer et al. (1991) using data from the gamma-ray spectrometer aboard *HEAO 3*, and by Sacco et al. (1990) using the FIGARO II balloon-borne experiment. However, with the launch of the *Compton Gamma Ray Observatory*, a positive detection in the 1–30 MeV range has been reported by the COMPTEL instrument team (Bennett et al. 1994; Schönfelder et al. 1994).

Geminga, long known as a bright, steady high-energy gamma-ray source, was first discovered to be a 0.237 s X-ray pulsar by Halpern & Holt (1992) using *ROSAT*. Once a period was known, pulsations at that period were also identified in EGRET (Bertsch et al. 1992), *COS B* (Bignami & Caraveo 1992), and *SAS 2* (Mattox et al. 1992) gamma-ray data. Geminga is unique among rotation-powered X-ray and gamma-ray pulsars in that, to date, no pulsed radio emission has been detected.

[1] strickman@osse.nrl.navy.mil.

The Geminga pulse profile at gamma-ray energies, observed by EGRET, exhibits a characteristic double peak structure with peak separation of ~0.5 in phase (Mayer-Hasselwander et al. 1994), compared to a separation of 0.42 for Vela (Kanbach et al. 1994). We define the first gamma-ray peak to be the one preceeding the interpeak emission. Peak FWHMs are a factor of ~2 wider in phase for Geminga than for Vela.

Measurements of Geminga at X-ray energies by *ROSAT* can be divided into soft and hard spectral components, as described by Halpern & Ruderman (1993). The light curve is energy dependent with the single broad peak observed below ~0.5 keV trailing the somewhat narrower single peak observed above ~0.5 keV by approximately 105° in phase.

Evidence exists that some, if not most, of the known gamma-ray pulsars have spectral breaks somewhere above 100 keV (see, e.g., Nel & De Jager 1993). Since the location of these breaks bears on models of the emission processes, studies of Vela and Geminga with OSSE may help better define the pulsar emission process.

The OSSE results we report in this paper help to elucidate spectral behavior of both these sources via a detection in the case of Vela and upper limits in the case of Geminga. In § 2, we discuss the nature of the observations made with OSSE. Section 3 elaborates on the analysis techniques used on the data from these observations. The results are presented in § 4 and discussed in § 5.

2. OBSERVATIONS

The OSSE instrument, described in detail by Johnson et al. (1993), consists of four independent phoswich scintillation detectors that operate in the 0.05–10 MeV range. Observations requiring high time resolution (better than ~8 s) are telemetry bandwidth limited; hence, for both the Vela and Geminga observations, high time resolution data are only available in relatively broad energy bands.

OSSE normally operates in an on-source off-source chopping mode in order to measure background. However, when observing a periodically pulsating source, the flux in the pulsations can often be estimated by comparing the on-pulse phase regions of the epoch-folded light curve to those off the pulse. Typically, the pulse profile is modeled in some fashion. The phase region not included in the model pulse is assumed to be background, and that flux level is subtracted from the remainder. In some cases, the phase region to be used for background determination is based on other criteria, for example, some previous measurement, perhaps at a different energy. In either case, only the spectrum of the pulsed component can be determined by OSSE in this mode. To measure unpulsed emission from the source, on-source off-source chopping must be performed, reducing on-source live time substantially (typically by a factor of 2). The Vela observations reported here were all performed in "staring" mode in which no chopping was performed. Of the Geminga observations, two had at least some detectors chopping, while one was performed entirely in the staring mode.

The OSSE detectors were used to observe the Vela pulsar on three occasions during the 2 year interval from 1991 August through 1993 August. The individual observations, referred to as viewing periods (VP), are described in Table 1. Note that the observation referred to as VP 26/28 was analyzed as a single observation even though it contained an 8 day gap during which Vela was not observed. Live times are given in detector-seconds (i.e., number of OSSE detectors observing times live time per detector). The observation parameters and pulsar ephemerides are listed in the table. In general, band boundaries were picked in order to avoid major background lines. Note that the 0.77–

TABLE 1

VELA PULSAR OBSERVATION SUMMARY

Viewing Period	Start	Stop	Pulsar Live Time (detector-seconds)	Bands[a]	Epoch T_0 (JD −2,440,000.5)	SSB Radio Phase at T_0 [b]	Frequency ν (s^{-1})	$\dot{\nu}$ (10^{-11} s^{-2})	$\ddot{\nu}$ (10^{-21} s^{-3})
8	91/8/22	91/9/5	8.08×10^5	1, 2, 3, 4	8504	0.034	11.1987003711301	−1.56791	4.17
26/28[c]	92/4/23	92/5/14	5.59×10^5	1, 2, 3, 4	8718	0.064	11.1984109503280	−1.56413	1.49
301	93/8/17	93/8/24	5.98×10^5	1, 2, 4	9228	0.403	11.1977224439102	−1.56079	−0.116
Total			1.96×10^6						

[a] Band 1: 0.07–0.19 MeV. Band 2: 0.22–0.61 MeV. Band 3: 0.76–2.0 MeV. Band 4: 2.0–9.7 MeV.
[b] Phase of photon arriving at SSB at time T_0, where radio peak is at phase 0.
[c] Vela not observed from April 29 through May 6.
NOTE.—Time resolution: 4 ms for all viewing periods.

TABLE 2

GEMINGA OBSERVATION SUMMARY

Viewing Period	Start	Stop	Pulsar Live Time (detector-seconds)	Chopped Source Live Time (detector-seconds)[a]	Epoch T_0 (JD −2,440,000.5)	EGRET Phase at T_0 [b]	Frequency ν (s^{-1})	$\dot{\nu}$ (10^{-13} s^{-2})	$\ddot{\nu}$
34	92/7/16	92/8/6	1.22×10^6	3.91×10^5	8750	0.02	4.21766909413	−1.95218	0
310	93/12/1	93/12/13	2.27×10^5	3.75×10^5	8750	0.02	4.21766909413	−1.95218	0
335[c]	94/7/12	94/8/1	7.72×10^5	none	8750	0.02	4.21766909413	−1.95218	0

[a] Detector-seconds on-source during chopping observation.
[b] Phase of photon arriving at SSB at time T_0, where EGRET "Peak 1" is at phase 0.
[c] Geminga not observed from July 19 through July 24.
NOTE.—Time resolution: 8 ms for all viewing periods.

2.0 MeV band, a region of high instrumental background, was not included in VP 301. Instead, the 2.0–9.7 MeV band was split into two bands. The results of these two bands have been combined here, both for compatibility with the previous observations and because no detection was made in the individual bands.

OSSE observed Geminga on three occasions from 1992 through 1994 (see Table 2). As indicated in the table, OSSE operated in chopping mode during the VP 34 and VP 310 Geminga observations, although two detectors were staring at Geminga during VP 34. Due to the configuration of the observation, the chopping mode result is very susceptible to systematic uncertainties. We are continuing evaluation of the effects and will report on the results of the chopping mode observations in a future paper. We used both the staring mode data and the chopping mode data during times when the detectors were pointed at the source for the Geminga pulsar analysis.

During the Geminga observations, OSSE acquired 8 ms rate samples in seven energy bands between 0.078 and 9.9 MeV. In order to improve statistics for the Geminga pulsar analysis, we have summed all the available data into two broad bands, 0.078–0.56 and 2.0–9.9 MeV (we had no data covering the gap between 0.56 and 2.0 MeV).

3. ANALYSIS AND RESULTS

3.1. *Epoch Folding Techniques*

The pulsed flux analysis consisted of phase-coherent summing (i.e., epoch folding) of 4 ms (Vela) or 8 ms (Geminga) rate samples to produce light curves for each viewing period and energy band. Mean arrival times at the solar system barycenter were computed for each rate sample (using the JPL DE200 ephemeris), and the phase of that sample was determined using a precise ephemeris. In the case of Vela, Taylor, Nice, & Azourmainian (1992) supplied a radio ephemeris as part of the *CGRO* pulsar monitoring program (see Table 1). For Geminga, the EGRET team (Mattox 1994) supplied a gamma-ray based ephemeris, which proved valid over a wide range of epochs (see Table 2). The ephemerides used were constructed to be valid for each of the viewing periods involved. Corrections were applied to account for a 2.042 s clock offset in the times supplied by the *CGRO* spacecraft during the first two Vela observations. Given these corrections, the ephemerides adequately predicted both period and peak absolute phase. We estimate period and event timing uncertainties to be ~ 0.2 ms for the determination of relative phase of the beginning of a given rate sample and ~ 0.4 ms for the absolute phase of the beginning of a rate sample relative to the radio or EGRET peak.

We epoch-folded each Vela and Geminga viewing period separately. For each rate sample, we computed the phase using the barycentric arrival time and the pulsar ephemeris, then summed rate samples into 22 bin phase histograms for Vela and 32 bin phase histograms for Geminga. Each phase bin thus represents approximately one time resolution unit. Since we had precise ephemeris information, we did not attempt to optimize any result by searching frequency space, nor did we attempt any optimization by varying phase bin widths or phases.

The epoch-folding process calculated phases relative to the center of the leading radio (Vela) or gamma-ray (Geminga) peak based on the previously cited ephemerides.

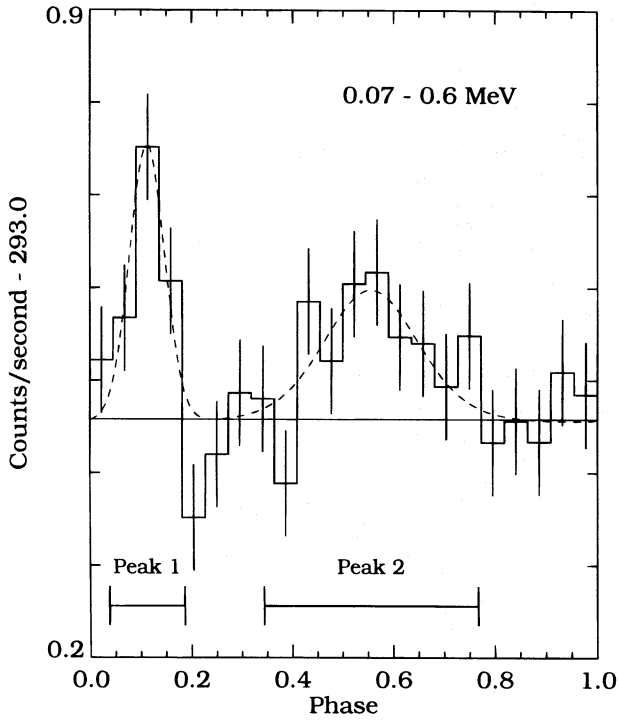

FIG. 1.—Vela pulsar light curve for the sum of viewing periods 8, 26/28, and 301, summed over the two lowest energy bands (0.07–0.6 MeV). The horizontal solid line is the background level computed from the off-peak regions. The dashed line is the best-fit circular normal function model of the pulse profile.

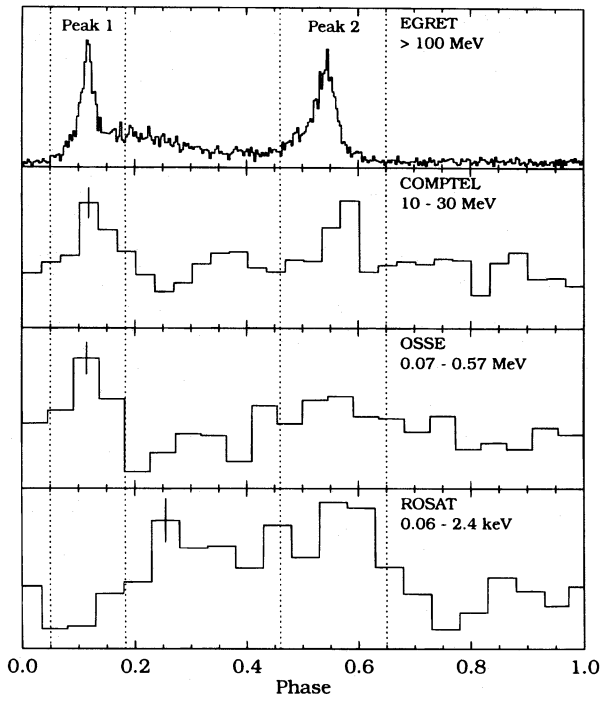

FIG. 2.—Vela pulsar light curves from *ROSAT* (Ögelman et al. 1993), OSSE, COMPTEL (Bennett et al. 1994), and EGRET (Kanbach et al. 1994), aligned in phase with the radio phase at 0.0. The dotted lines show the EGRET peak regions.

TABLE 3

VELA PULSAR PULSED FLUX SUMMARY

Band[a]	Viewing Period	Peak 1 Flux[b]	Peak 2 Flux[b]	Peak 1+2 Flux[b]
0.07–0.6[c]	VP 8	120 ± 30	180 ± 60	310 ± 80
	VP 26/28	90 ± 30	60 ± 70	150 ± 90
	VP 301	50 ± 40	80 ± 70	120 ± 90
	VP 8 + 26/28 + 301	90 ± 20	120 ± 40	210 ± 50
0.07–0.19.....	VP 8	190 ± 80	240 ± 160	430 ± 200
	VP 26/28	180 ± 90	60 ± 180	240 ± 230
	VP 301	210 ± 90	380 ± 190	580 ± 230
	VP 8 + 26/28 + 301	190 ± 50	230 ± 100	420 ± 130
0.22–0.6	VP 8	99 ± 31	167 ± 65	267 ± 81
	VP 26/28	61 ± 37	62 ± 76	123 ± 95
	VP 301	−7 ± 37	−19 ± 76	−26 ± 95
	VP 8 + 26/28 + 301	57 ± 20	83 ± 41	140 ± 52
0.76–2.0	VP 8	−8 ± 14	−30 ± 30	−38 ± 38
	VP 26/28	7 ± 16	−6 ± 34	0.7 ± 43
	VP 301	...	...	...
	VP 8 + 26/28	−2 ± 11	−20 ± 22	−22 ± 28
2.0–9.7	VP 8	0.7 ± 1.5	5.6 ± 3.1	6.2 ± 3.9
	VP 26/28	1.7 ± 1.8	0.6 ± 3.7	2.3 ± 4.6
	VP 301	−1.4 ± 1.8	5.1 ± 3.6	3.6 ± 4.5
	VP 8 + 26/28 + 301	0.3 ± 1.0	4.0 ± 2.0	4.3 ± 2.5

[a] Bands in MeV.
[b] 10^{-6} photons cm^{-2} s^{-1} MeV^{-1}, phase averaged.
[c] Note that this is the concatenation of the next two bands.

For Vela, phase 0.0 (the lower edge of the first phase bin) for each light curve is the centroid of the radio peak. For Geminga, phase 0 is the nominal centroid of EGRET peak 1.

The analysis produced phase histograms of counts and live time for each energy band. Since we constructed the phase histograms such that the absolute phase of each bin relative to the above-mentioned features remained the same for all observations, we were able to coherently sum the histograms from the three viewing periods. To characterize light curve features with optimum sensitivity, we summed phase histograms from several energy bands together. These were normalized by live time (phase bin by phase bin) and energy bandwidth for modeling and display purposes.

3.2. *Vela Light Curve*

We have detected pulsed emission from Vela during all three observations (albeit at low statistical significance in VP 301; see Table 3). Figure 1 shows the light curve summed over all the viewing periods and the two lowest energy bands (0.07–0.6 MeV overall) . The horizontal line represents the average flux from the off-pulse or background phase regions as described in the previous section. Figure 2 shows the OSSE light curve compared to other measurements at lower and higher energies.

In order to determine on-pulse and off-pulse light curve regions, we fitted the sum of the two low-energy band light curves with a model consisting of a constant background and two peaks represented by circular normal functions. The circular normal function is defined by the relation

$$F = \frac{A}{I_0(k)} e^{k \cos [2\pi(x - x_c)]},$$

where A controls the peak amplitude, k is the "compactness," which is inversely related to the peak width, x_c is the phase of the center of the peak, and I_0 is the modified Bessel function of order zero. The circular normal function has the property that, although it is roughly Gaussian in shape, it is periodic in phase with period 1. Hence, it is well suited to modeling light curve peaks that "wrap around" the phase histogram. All parameters in the peaks and background were free to vary. We used these models to determine peak positions and widths, but not peak amplitudes, as described below. The resulting peak positions and widths are listed in Table 4.

We defined the "peak" or "on-source" phase regions as the regions of the light curve within the full width at 10% maximum of the two best-fit peak models. Since we saw no evidence for any other significant excesses, the remainder of the light curve was treated as unpulsed emission and used to determine background for spectral analyses. For each energy band, the background regions in the original count and live-time histograms were summed, normalized by the ratio of the live time from the peak region to that from the background region, and subtracted from the total counts from the peak region. The resulting difference, still in counts, was then normalized by the total live time for the entire light curve, resulting in a phase-averaged peak rate. This technique is preferable to using the circular normal function peak amplitudes to provide peak fluxes, since it is not as vulnerable to misrepresentation of the data by the model and is more straightforward for uncertainty calculation.

The significance of the detection was determined using the maximum likelihood ratio technique described by Li &

TABLE 4

VELA PULSAR PULSE PROFILE MODEL BEST-FIT PARAMETERS[a]

Parameter	Value
Peak 1 Phase	$0.11^{+0.02}_{-0.01}$
Peak Separation.....	0.44 ± 0.06
Peak 1 FWHM	$0.08^{+0.05}_{-0.04}$
Peak 2 FWHM	$0.22^{+0.25}_{-0.16}$

[a] All parameters are in units of folded light curve phase (0.0–1.0).

TABLE 5

VELA PULSAR MAXIMUM LIKELIHOOD RATIO (MLR) TEST SUMMARY

Viewing Period	Peak 1 MLR	Peak 2 MLR	Peak 1+2 MLR
VP 8	2.9×10^{-5}	1.3×10^{-3}	4.0×10^{-5}
VP 26/28	6.2×10^{-3}	2.0×10^{-1}	4.9×10^{-2}
VP 301	1.3×10^{-1}	1.7×10^{-1}	1.1×10^{-1}
VP 8 + VP 26/28 + VP 301	2.4×10^{-6}	1.7×10^{-3}	2.1×10^{-5}

Ma (1983) applied to the summed fluxes in the "source" and "background" regions. The source region is defined to be the sum of the two peak regions, while the background region is everything else. The distribution of counts in the background region can be represented by expectation value $\langle N_B \rangle$, while the distribution of counts in the source region is $\langle N_S \rangle + \alpha \langle N_B \rangle$, where $\langle N_S \rangle$ is the expectation value of the number of excess pulsed counts from the source and $\alpha = t_S/t_B$ is the ratio of source region to background region live times. The test computes a ratio of the maximum likelihoods in which the numerator is the likelihood of obtaining the observed results given the null hypothesis $\langle N_S \rangle = 0$. The denominator is the maximum likelihood of obtaining the observed results given that $\langle N_S \rangle$ can be nonzero. Li & Ma have shown that $S = (-2 \ln \lambda)^{1/2}$ (where λ is the likelihood ratio) is distributed as the absolute value of a standard normal variable (i.e., zero mean and unit variance). The probability (as shown in Table 5) of obtaining a value of S equal to or greater than the one observed tests the null hypothesis. A small probability means that the null hypothesis can be rejected with some confidence, i.e., that there is a significant excess (or deficiency) of counts in the pulse region.

Table 5 displays the matching results of the maximum likelihood ratio (MLR) test for each peak and viewing period summed over the two lowest energy bands.

The overall MLR significance of detection of the first gamma-ray pulse profile peak integrated over all three observations is $\sim 4.6\ \sigma$ in the sum of the two lower energy bands. We detect the second gamma-ray peak at only marginal significance ($\sim 3\ \sigma$) in the same band. Although Table 5 gives the impression that we did not detect the pulsar at all during VP 301, note that this table represents data in the sum of the two lower energy bands (0.07–0.6 MeV). Comparing detections in the lowest band alone (0.07–0.19 MeV) in Table 3, we see that VP 301 did indeed contribute to the overall detection significance.

We see no significant evidence of temporal variability in either peak or any of the energy bands. Table 6 shows the results of computing χ^2 assuming a constant flux model (with flux equal to the mean) for each peak. For none of the combinations of peaks and bands can the constant flux (i.e., no temporal variability) model be rejected with as much as 95% confidence (the probability of observing the data with a constant model assuming random fluctuations is given in parentheses in the table). Although the source is not detected in the 0.22–0.6 MeV band during VP 301 (note the higher χ^2-values in that band), the resulting flux decrease is not significant, as indicated by the probabilities of random fluctuations producing the observed χ^2. In addition, we have compared light curves for each band between pairs of viewing periods (subtracting the background in each case) and see no evidence for significant variability. For the remainder of this discussion, we will treat the sum of the three viewing periods only.

The light curve looks qualitatively similar to the light curves measured at higher energies (Buccheri et al. 1978; Grenier et al. 1988; Kanbach et al. 1994). We have characterized our observed light curve shape via a model as mentioned above. The results of this characterization (for the optimal-sensitivity 0.07–0.60 MeV band) are displayed in Table 4 and plotted in Figure 1. OSSE measures a first peak width of $0.08^{+0.05}_{-0.04}$ in phase in the 0.07–0.60 MeV band. The EGRET first peak is ~ 0.03 wide in phase, which, although narrower, is not statistically inconsistent with the OSSE result. The second peak appears to be almost a factor of 3 broader than the first, as opposed to EGRET observations, which indicate that the second peak is ~ 1.7 times broader than the first above 100 MeV (Kanbach et al. 1994). However, not only is the width of the second peak not well determined (as indicated in Table 4), but the F-test for models with and without the second peak indicates that it is only required at the $\sim 2.6\ \sigma$ level. Hence, although we have an indication that the second peak is broader than the first, we cannot make this claim with confidence. The positions of the OSSE peaks, as represented by the best-fit model, are consistent with the EGRET peak positions given in Kanbach et al. (1994).

3.3. *Geminga Light Curve*

We have analyzed the Geminga data for pulsed emission in a fashion similar to Vela, using ephemerides provided by the EGRET team (Mattox 1994). We saw no evidence of pulsations in either the low- or high-energy bands in the individual observation light curves nor in the light curve representing the sum of the three observations. The latter are shown in Figure 3. The EGRET 30–100 MeV light curve, also shown in this figure, is taken from Mayer-Hasselwander et al. (1994). It has been phase aligned with the OSSE light curve using the relative epochs and phases. Note that the phase axis has been shifted such that the zero of phase, which in this representation corresponds to the centroid of the first EGRET peak,[2] is in the middle of the figure.

We can demonstrate in several ways that there is no statistically significant evidence for peaks in the Geminga light curve. First, if we simply compute the pulsed flux in the EGRET peak regions, using for background the phase regions not included in the EGRET peaks, we see no evidence of significant excess. Further, assuming that the data are represented by the mean, we calculate χ^2. For the low-energy band, $\chi^2/\mathrm{dof} = 1.33$ for 31 dof. The probability of observing this value or higher given only random fluctuations about the constant mean is 0.10. A similar calculation for the high band gives $\chi^2/\mathrm{dof} = 0.91$ with a probability of

[2] The phase axis is referenced to the nominal EGRET peak as defined by the EGRET ephemeris. This may differ slightly from the peak displayed in the figure, since the peak position varies slightly with energy.

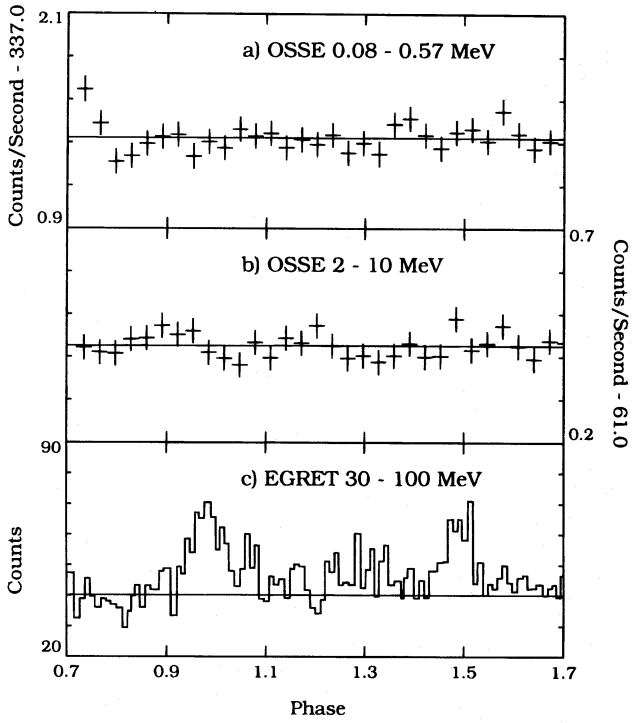

FIG. 3.—Geminga light curves for the sum of VP 34, VP 310, and VP 335 and two energy bands, together with 30–100 MeV EGRET light curve from Mayer-Hasselwander et al. (1994).

0.60. Hence, we cannot reject the hypotheses that the parent distributions are independent of phase.

Next, we have computed the Li & Ma (1983) MLR for the positions of each EGRET peak. In no case (i.e., peak 1, peak 2, or both peaks in either energy band) can we reject the null hypothesis of zero source counts with better than 1.5 σ (87%) confidence. In addition, we have examined the first half of the EGRET interpulse 2 (I2) region (the interpulse region with less flux), since this region has the softest EGRET spectrum and the first half of the region appears to be the source of the flux in the 30–100 MeV light curve. We cannot reject the null hypothesis for this phase region to any better than 0.6 σ.

ROSAT observations of pulsed emission from Geminga (Halpern & Holt 1992; Halpern & Ruderman 1993) have demonstrated, in the 0.5–1.5 keV band, a peak in the light curve between EGRET peaks 1 and 2. Halpern (1995) has indicated that the absolute phase of the *ROSAT* light curve relative to the EGRET light curve, as shown in Figure 2 of Halpern & Ruderman (1993) is not reliable. Therefore, we have not attempted to phase align this result with the OSSE light curves.

TABLE 6

VELA PULSAR PULSED FLUX VARIABILITY TEST SUMMARY

Band[a]	χ^2/dof Peak 1[b]	χ^2/dof Peak 2	χ^2/dof Peak 1+2
0.07–0.6[c]	1.51 (0.22)	1.15 (0.32)	1.61 (0.20)
0.07–0.19.....	0.02 (0.98)	0.77 (0.47)	0.56 (0.57)
0.22–0.6	2.41 (0.09)	1.84 (0.16)	2.78 (0.06)
2.0–9.7	0.82 (0.44)	0.63 (0.54)	0.23 (0.79)

[a] Bands in MeV.

[b] Tests hypothesis that individual viewing periods are randomly distributed about the mean of all the viewing periods; number in parentheses is probability ($\chi^2 > \chi^2_{obsvd}$).

[c] Note that this is the concatenation of the next two bands.

3.4. *Vela Spectrum*

We used a forward-folding process to compare the data to various model spectra. In this procedure, a model spectrum was folded through the instrument response and the resulting model count rate spectrum was compared to the data in a χ^2 sense. The model spectra and responses were created and multiplied in narrow energy bands, then integrated over the broad OSSE bands so that spectral variations over each band, appropriately weighted by response, were accounted for. The fitting routine used was based on the Marquardt algorithm with data points weighted by their uncertainties. The routine used no special treatment for upper limits (i.e., insignificant data points were treated like all the rest). The model parameters were varied until a model that generates a minimum χ^2 was determined. Since our background counting rates were high and energy bands broad, this was also guaranteed to be a maximum likelihood estimate. Parameter uncertainties were determined by χ^2-mapping using a procedure based on that described by Lampton, Margon, & Bowyer (1976).

Data from other experiments (e.g., EGRET and COMPTEL) were fitted simultaneously with OSSE spectra using the same forward folding technique. However, since we did not possess instrument responses for these data sets, published photon spectra were used and unit responses assumed. The model spectrum was still integrated over each band, but weighting by response within a band was not possible, so the results are somewhat approximate and should be viewed qualitatively.

We generated photon spectra from the data by multiplying each data point in the count spectrum by the ratio of the best-fit model photon spectrum to the best-fit model count spectrum. The resulting spectrum was dependent on the model chosen, although in the case of the Vela pulsar, the uncertainty in the result due to model dependence was small relative to the statistical uncertainty. The resulting photon spectra are compiled in Table 3.

Figure 4 displays the sum of the first and second peak emission (i.e., the difference of peak region and off-peak or background region rates). In order to compress the display in the OSSE energy range, the spectrum is plotted as $\langle E \rangle \times$ photon flux (i.e., an energy flux), where $\langle E \rangle$ is defined as the mean band energy, computed by averaging the energy weighted by a representative spectrum model over each band. Note that we use this scheme strictly for dynamic range compression in the plot. All of our models are specified as photon spectra, according to common practice in this energy range. Fluxes are normalized by division by the total live time and are, hence, time-averaged rather than instantaneous values. Data points less than one standard deviation above zero have been plotted as 2 σ upper limits (that is, two standard deviations above zero).

The spectrum is rather hard, particularly below 0.60 MeV. The OSSE spectrum is well represented by a single power law (see Fig. 5 for parameter confidence contours). The best-fit power-law index for the sum of both peaks is -1.3 ± 0.2, while the best-fit index for peak 1 is $-1.5^{+0.2}_{-0.3}$ and for peak 2 is -1.1 ± 0.2. Note that the uncertainty for peak 2 is comparable to that for peak 1 even though peak 1 appears more significant in Table 5. This is because the table is computed for the sum of the two lower energy bands, where peak 1 is strongest, while a significant portion of the peak 2 flux comes from the highest energy band (see

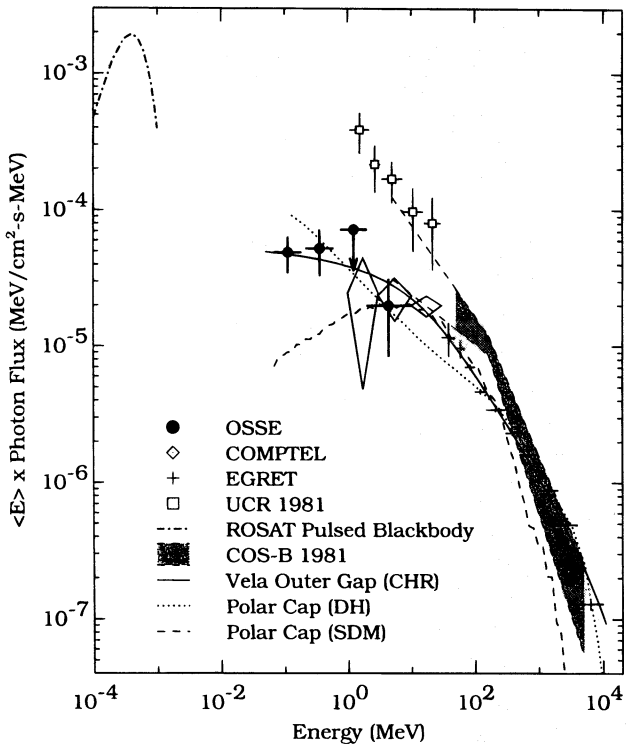

FIG. 4.—Vela pulsar spectrum for the sum of viewing periods 8, 26/28, and 301. Flux is the sum of both peaks, background subtracted and averaged over the entire light curve. It is presented as $\langle E \rangle \times$ photon flux. Upper limits are 2 σ above zero. The data and models displayed are EGRET (Kanbach et al. 1994); COMPTEL (Schönfelder et al. 1994); UCR (Tümer et al. 1984); *COS B* 1981 best-fit two power-law model (Grenier et al. 1988); *ROSAT* (Ögelman et al. 1993); Vela Outer Gap Model (Cheng et al. 1986); and Polar Cap Models (DH, Daugherty & Harding 1996; and SDM, Sturner et al. 1996). The Vela Outer Gap Model has been adjusted in shape and normalization to fit the data, while the Polar Cap Models have been normalized only. The shaded region represents the actual *COS B* energy range, while the dashed lines extrapolate the *COS B* spectrum to lower energies.

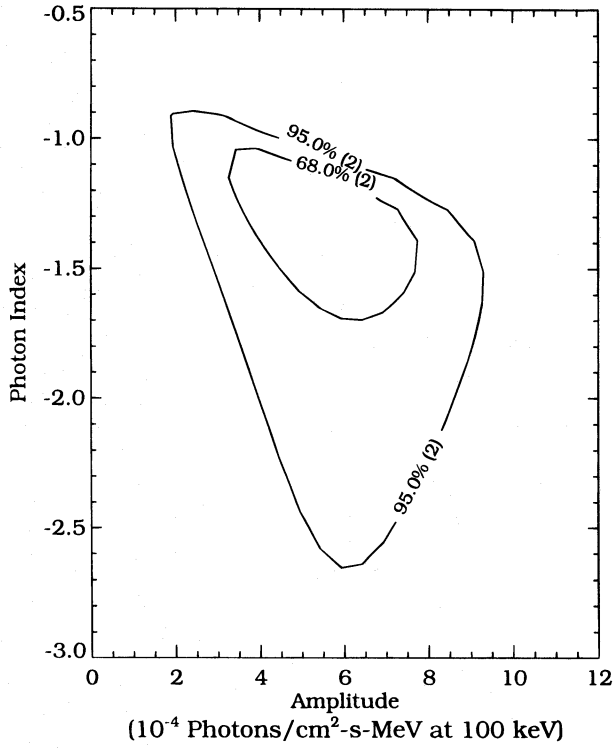

FIG. 5.—Confidence contours for a single power-law fit to the OSSE Vela pulsar spectrum (peaks 1+2). Confidence intervals and number of interesting parameters are indicated on the contours. Intervals are determined using the prescription of Lampton et al. (1976).

Table 3), which is not included in the computation of MLR. The peak 1 and peak 2 results are consistent with each other to within statistics. The OSSE result thus contains no evidence of phase-dependent spectral shape. We will discuss several other models for the data in § 4.

3.5. *Geminga Spectrum*

In the case of Geminga, in which no significant pulsations were observed, we used the following formula from Ulmer et al. (1991), to compute upper limits:

$$\mathrm{UL} = \frac{N\sqrt{C_{\mathrm{tot}}}}{\Delta E A_{\mathrm{eff}} t}\sqrt{\frac{\beta}{1-\beta}} ,$$

where N is the confidence level for the upper limit in units of standard deviation (taken to be 2), β is the pulsar duty cycle, C_{tot} is the total number of counts in the light curve, ΔE is the energy band, A_{eff} is the effective area integrated across that band, and t is the live time. For a pulsar duty cycle, we have used 0.5 (the most conservative choice). Although the EGRET peaks are much narrower than this, *ROSAT* Halpern & Ruderman (1993) and COMPTEL (Kuiper et al. 1995) report different light curve shapes and peak locations, making prediction of the light curve shape in the OSSE band difficult.

Figure 6 displays the OSSE upper limits computed as described above, together with a spectrum measured by COMPTEL (Kuiper et al. 1995) and the EGRET total pulsed spectrum together with an extrapolation of the EGRET best-fit power-law model to lower energies (Mayer-Hasselwander et al. 1994).

Although not plotted in the figure, we have also considered the OSSE upper limits for the first half of the EGRET I2 region as discussed above. These are lower than the plotted limits by the ratio of the

$$\sqrt{\frac{\beta}{1-\beta}}$$

terms in the upper limit expression, where this term is equal to 1 for $\beta = 0.5$ and is equal to 0.5 for $\beta = 0.2$, the duty cycle for the first half of the I2 region. Hence, the upper limits for this phase assumption are lower by a factor of 2 than those shown.

4. DISCUSSION

The Vela light curve as measured by OSSE is roughly similar to the light curve observed at higher energies (see Fig. 2). However, we observe weak evidence that the second peak could be somewhat broader than that observed, for example, by EGRET. Hence, the OSSE data may serve as a bridge between the high-energy data and the light curve measured at X-ray energies by *ROSAT* (Ögelman et al. 1993). The latter has a broad, complex pulse centered at a phase of ~ 0.7 relative to the radio pulse. A broad second pulse in the X-ray band has been predicted by Romani & Yadigaroglu (1994).

The emerging picture of the Vela pulsed spectrum consists of a hard spectrum at low gamma-ray energies, breaking to a rather softer spectrum at higher energies (Fig. 4). The EGRET and COMPTEL spectra are total pulsed flux

in each case. Fitting a power-law model to OSSE, COMPTEL (Schönfelder et al. 1994), and EGRET (Kanbach et al. 1994) data results in an unacceptably high χ^2/dof (39 for 16 degrees of freedom). Using, instead, a broken power-law model requires a break between the two power-law components at 26 ± 8 MeV. The broken power-law model results in a χ^2/dof of 7.7 for 14 degrees of freedom, better than the single power law but still not very good. Since the actual spectral shape may roll over smoothly rather than with an abrupt break, the break energy of the broken power law is only a rough indication of spectrum behavior and may be dependent on the energy range used in the fit. If we perform the same fit to OSSE, COMPTEL, and EGRET peaks 1 and 2 data separately, relatively poor OSSE and COMPTEL statistics do not allow us to rule out the same break energy and magnitude to each peak, or to the sum of the peaks.

The X-ray spectrum displayed in Figure 4 is the single blackbody model that best represents the pulsed emission observed by *ROSAT* (Ögelman et al. 1993). There has been no report of a hard component in the pulsed emission, although such a component has been suggested by Ögelman (1993) for the total emission from the point source. Bridging the gap between the *ROSAT* and OSSE observations could confirm the details of the magnetospheric gamma-ray emission at low energies, where modeling is difficult. This should be a high priority for observations of Vela during future missions.

Figure 4 displays three theoretical model spectra for pulsed emission from Vela. The Vela outer gap model (Cheng, Ho, & Ruderman 1986; Ho 1993), and two polar cap emission models (Daugherty & Harding 1996, labeled DH; and Sturner, Dermer & Michel 1996, labeled SDM) represent the data with varying degrees of success. The only model with a significant disagreement in the OSSE band is the last, which rolls over to a spectrum that is too hard below 1 MeV and too soft in the EGRET energy range. We emphasize that the poor agreement with the data of the two polar cap models compared to the outer gap model is somewhat misleading, since the outer gap model, an analytic function with three free parameters, was actually fit to all the data, while the other two, available only in tabular form, were normalized only.

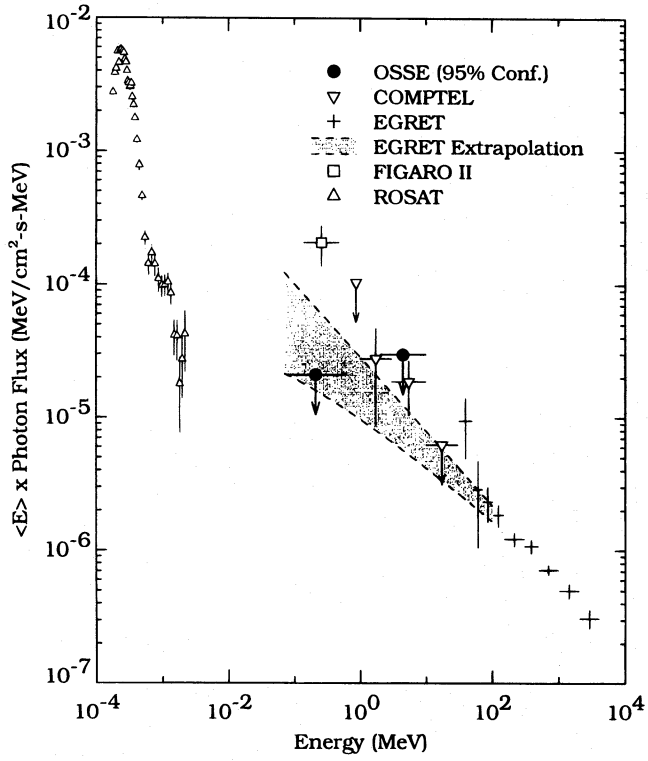

FIG. 6.—Geminga spectral upper limits from OSSE and COMPTEL, together with an extrapolation of the EGRET best-fit power-law model. Also, the reported pulsed flux from FIGARO II (Sacco et al. 1990).

The Vela outer gap model, as used here, has two parameters in addition to normalization. These are E_{max}, the maximum secondary synchrotron photon energy, and $u_{min} = \gamma_{min}/\gamma_{max}$, where γ_{max} is the maximum energy achieved by electrons in the gap accelerator and γ_{min} is the low-energy cutoff in the electron spectrum caused by electrons escaping across the light cylinder before losing all their energy to synchrotron radiation. The radiation spectrum is a smoothly varying power law from $E_{min} = u_{min}^2 \times E_{max}$ to E_{max}. Below E_{min}, the spectrum should harden, with $E^{-2/3}$ the hardest possible spectrum expected (Ho 1993). Fitting the outer gap model to OSSE, COMPTEL and EGRET data results in $E_{max} = 41 \pm 12$ GeV and $u_{min} = 0.021 \pm 0.008$, which leads to $E_{min} = 18$ MeV. The latter is consistent with the break energy found using a broken power-law model. A simple power-law fit to the OSSE data alone has a best-fit index of -1.3 ± 0.2, which is softer than the hardest predicted index of $-\frac{2}{3}$ and, hence, does not reject these models on the basis of exceeding the maximum hardness. Note that the best-fit Vela outer gap model does not represent the high-energy cutoff present in the EGRET spectrum at ~ 4 GeV. This is not surprising given the best-fit value for E_{max} of 41 GeV. If E_{max} is lowered to produce a cutoff at the lower energy, the modeled cascade produces insufficient photons in the OSSE energy range.

Tümer et al. (1984) have reported a detection of pulsed emission from Vela in the range 0.3–30 MeV based on a balloon flight in 1981 November. Their results are shown in Figure 4. Their reported fluxes are significantly higher and perhaps softer than those measured by the *CGRO* instruments; however, contemporaneous measurements by *COS B* in 1981 (Grenier et al. 1988) were also soft compared to the EGRET measurements, which, according to Kanbach et al. (1994), have shown no evidence of variability from 1991 May through 1992 November. Figure 4 shows that an extrapolation of the *COS B* spectrum below 300 MeV is still marginally too low to explain the UCR result, although a downward extrapolation of the spectrum above 300 MeV would intersect the Tümer result reasonably well. The coincidence of both 1981 measurements being higher than the *CGRO* results hints at long-term variability in the Vela pulsed flux.

The Geminga spectrum (Fig. 6) in low-energy gamma rays is not as well determined as for Vela. The OSSE 2 σ upper limit from 0.08–0.6 MeV is low compared to the extrapolation of the EGRET best-fit spectrum, as shown here with an extrapolated 68% confidence region (Mayer-Hasselwander et al. 1994). However, the disagreement is not very significant. If we integrate the EGRET extrapolation over the lower OSSE band, it disagrees with the OSSE null detection by ~ 1.5 σ, a result almost entirely driven by the uncertainty in the EGRET extrapolation. The COMPTEL result is also more or less consistent with the EGRET extrapolation. Therefore, we cannot insist on a break in the

spectrum similar to that observed in Vela. However, the spectrum must break somewhere in order not to exceed the *ROSAT* flux. The break cannot be much below 10 keV without requiring an unreasonably hard spectrum below the break, and it cannot break much above 3 MeV without contradicting the COMPTEL result. The OSSE upper limit disagrees strongly with the claimed detection by FIGARO II (Sacco et al. 1990).

5. SUMMARY

OSSE observations of the Vela and Geminga pulsars have detected the former and set significant upper limits on the spectrum of the latter in the low-energy gamma-ray range. In both cases, OSSE (and COMPTEL) results, when extrapolated up in energy, require (or, in the case of Geminga, suggest) a break to a softer spectrum in order to intersect EGRET data above 70 MeV. For Vela, this break appears in the 20–30 MeV range, while for Geminga it is not well determined. The Vela pulsar light curve measured by OSSE is similar to that at higher energies, within the limited statistics of the OSSE detection. The Vela pulsed spectrum in the OSSE range is quite hard, although not so hard that it violates constraints of synchrotron production models. The data are well represented by an outer gap model, but polar cap models are not firmly excluded.

The authors would like to thank Cheng Ho, Alice Harding, and Steve Sturner for making software and/or tabular implementations of their respective models available to us, along with useful discussions concerning these models. In addition, we greatly appreciate the COMPTEL and EGRET teams supplying us with their data in numerical form. This work was supported by NASA contract S-10987-C.

REFERENCES

Bennett, K., et al. 1977, A&A, 61, 279
Bennett, K., et al. 1994, ApJS, 90, 823
Bertsch, D. L., et al. 1992, Nature, 357, 306
Bignami, G. F., & Caraveo, P. A. 1992, Nature, 357, 287
Buccheri, R., et al. 1978, A&A, 69, 141
Cheng, K. S., Ho, C., & Ruderman, M. 1986, ApJ, 300, 522
Daugherty, J., & Harding, A. 1996, in preparation
Grenier, I. A., Hermsen, W., & Clear, J. 1988, A&A, 204, 117
Halpern, J. P. 1995, private communication
Halpern, J. P., & Holt, S. S. 1992, Nature, 357, 222
Halpern, J. P., & Ruderman, M. 1993, ApJ, 415, 286
Ho, C. 1993, in Isolated Pulsars, Proc. Los Alamos Workshop, ed. K. A. Van Riper et al. (Cambridge: Cambridge Univ. Press), 271
Johnson, W. N., et al. 1993, ApJS, 86, 2
Kanbach, G., et al. 1994, A&A, 289, 855
Kuiper, L., et al. 1995, A&AS, in press
Lampton, M., Margon, B., & Bowyer, S. 1976, ApJ, 208, 177
Li, T., & Ma, Y. 1983, ApJ, 272, 317
Mattox, J. R. 1994, private communication
Mattox, J. R., et al. 1992, ApJ, 401, L23
Matz, S. M., et al. 1994, ApJ, 434, 288
Mayer-Hasselwander, H. A. 1994, ApJ, 421, 276
Nel, H. I., & De Jager, O. C. 1993, in Proc. Second Compton Symp., ed. C. E. Fichtel et al. (New York: AIP), 91
Ögelman, H. 1993, in Lives of Neutron Stars, ed. M. A. Alpar et al. (Dordrecht: Kluwer), 101
Ögelman, H., Finley, J. P., & Zimmermann, H. U. 1993, Nature, 361, 136
Romani, R. W., & Yadigaroglu, I. A. 1995, ApJ, 438, 314
Sacco, B., et al. 1990, ApJ, 349, L21
Schönfelder, V., et al. 1994, paper presented at 17th Texas Symp. on Relativistic Astrophysics
Sturner, S., Dermer, C. D. & Michel, C. 1996, in preparation
Taylor, J., Nice, D., & Azourmainian, Z. 1992, *GRO*/Radio Timing Database, maintained by Princeton University
Thompson, D. J., Fichtel, C. E., Kniffen, D. A., & Ögelman, H. B. 1977, ApJ, 214, L17
Tümer, O. T., Dayton, B., Long, J., O'Neill, T., Zych, A., & White, S. 1984, Nature, 310, 214
Ulmer, M. P., et al. 1994, ApJ, 432, 228
Ulmer, M. P., Purcell, W. R., Wheaton, W. A., & Mahoney, W. A. 1991, ApJ, 369, 485
Wallace, P. T., et al. 1977, Nature, 266, 692